**Proceedings of the ASME 2016 35th International Conference on Ocean, Offshore and Arctic Engineering**
**OMAE2016**
**June 19-24, 2016, Busan, South Korea**

# OMAE2016-54987

# CFD CALCULATIONS OF THE VORTEX-INDUCED MOTIONS OF A CIRCULAR-COLUMN SEMI-SUBMERSIBLE

**Guilherme Feitosa Rosetti** *
Numerical Offshore Tank - TPN
Dept. of Naval Architecture
and Ocean Engineering
University of São Paulo
São Paulo, Brazil
gfeitosarosetti@usp.br

**Rodolfo Gonçalves**
Numerical Offshore Tank - TPN
Dept. of Naval Architecture
and Ocean Engineering
University of São Paulo
São Paulo, Brazil
afujarra@usp.br

**André Luís Condino Fujarra** †
Numerical Offshore Tank - TPN
Dept. of Naval Architecture
and Ocean Engineering
University of São Paulo
São Paulo, Brazil
afujarra@usp.br

**Arjen Koop**
Offshore Department
MARIN
Wageningen, the Netherlands
a.koop@marin.nl

## ABSTRACT

*The vortex-induced motions (VIM) of offshore platforms stand as an intriguing and challenging engineering problem, drawing attention from industry, universities and research institutes. Field observations, model tests and calculations have extensively showed that the complex fluid-structure interaction can result in appreciable motions and increased fatigue of mooring and risers. It is thus a very relevant issue from the engineering standpoint. A large volume of experimental research has been carried out, mainly to verify designs and characterize the occurrence of VIM. Conversely, the numerical investigations applying CFD tools have shown to be a more flexible approach enabling better understanding of the physics at play due to the possibility of investigating the effects of different parameters upon the vortex induced motions of floating platforms. Moreover, the CFD calculations enable investigation of the full-scale behavior of the platforms under VIM, a very controversial issue presently. Bearing upon these issues, the VIM Joint Industry Project aims at increasing physical insight of this phenomenon by means of investigating the influence of geometric design variations, flow conditions and scale effects with the objective of improving practical knowledge that can be applied in the design stage of floating platforms. In this paper, we present some of the CFD studies, results and observations carried out within the JIP, regarding the VIM of a semi-submersible with circular columns in 0 and 45 degrees and over a wide range of reduced velocities. It is confirmed that the 0 degree incidence results in larger motions than the 45 degrees-incidence case, in contrast to the VIM behavior of a semi-submersible with square columns. The tests campaign carried out at the University of São Paulo for the same platform agree with these results. Within the lock-in range, the frequency synchronization of the lift forces on columns and pontoons cause*

*Currently, also at Argonáutica Engineering & Research.
†Currently, at Federal University of Santa Catarina (UFSC).

*large net transverse forces. Appreciable sway motions thus result. For larger reduced velocities, synchronization of the flow around the columns cease, but the forces on the pontoons then largely contribute to the total force. In this high-reduced velocity range, the phasing between total force and motion is such that energy transfer from the fluid to the body occurs, causing the amplification of the motions.*

## INTRODUCTION

The VIM of multi-column offshore platforms is a relevant issue in the design and operation of these structures. Stable and appreciable motions can occur when the force oscillations on its columns and pontoons are synchronized with the natural periods of the floater. That can have important consequences for the fatigue of mooring chains and risers and even extreme events have been pointed out as relevant [1].

Model tests have been for many years the main approach to study and predict VIM of offshore platforms, however field observations have shown that model tests results seem to overpredict motions [2]. As a consequence, floater design might be overly conservative considering these results, as commented in [3].

If one is to tackle this problem numerically, such complex fluid-structure interaction phenomenon requires a robust CFD code and considerable computational power to allow for large grids and long computational runs. Furthermore, verification and validation activities are recommended. The intricate interaction of vortices shed from multiple columns require refined grids, especially near the walls and in the near wake. The free motions, either in deforming or moving grids also bring up complexity, as pointed out by [4]. On the other hand, investigation on the sensitivity of geometrical details and other parameters, as well as full scale effects is possible and convenient with CFD, fully justifying its application.

Bearing upon these observations, MARIN and the University of São Paulo (USP) initiated the VIM Joint Industry Project to investigate possible candidates for this reduction in VIM response in the field. The main objectives of the VIM JIP were:

- Increase insight in physics and phenomenon behind VIM;
- Evaluate possible candidates for differences between model tests, CFD and field observations;
- Put most promising candidates to the test in model tests and CFD;
- Build confidence in CFD for VIM through dedicated verification and validation;
- Provide general conclusions and lessons learnt for VIM model tests and VIM CFD calculations.

The CFD code ReFRESCO [5] and model tests are used in this JIP in a complementary way: model tests [6] are used as reference for the CFD computations [7], allowing more thorough investigation and understanding of the flow dynamics, fluid structure interaction and full scale behavior. Floaters with squared and circular columns, different roughness and external damping levels, headings, draft variations and presence of waves have been considered in order to clarify VIM reduction observed in the field.

In the present paper, we present CFD calculations and studies carried out within the JIP, regarding the VIM of a semi-submersible with circular columns in 0 and 45 degrees and over a wide range of reduced velocities in model scale (full scale behavior will be addressed in a future publication). The experimental results of the same case is presented in [6]. We will present an investigation of loads and motions, added mass and damping for each reduced velocity in order to understand what drives large, steady motions within and out of the lock-in range. Special attention is given to the study of synchronization and phases of forces and motions with the objective of understanding the fluid-structure interaction mechanism at play.

The paper is organized as follows: the next section presents definitions of some parameters and conventions used throughout the paper; after that we briefly present some details of the model test campaign carried out with the same model; the details of the calculations are presented in the following section; a comparison of the decay results from calculations and model tests is then presented, after which the results and analysis of the VIM calculations in comparison with the model tests results are showed; finally, the last section draws some conclusions and perspectives of this work.

## CONVENTIONS AND DEFINITIONS

### Incidence Direction

The incidence convention follows the depicted plot in figure 1. For 0 degrees incidence, the flow is aligned with the global x-direction and columns 1 and 4 are upstream of 2 and 3. In the 45 degrees incidence, column 4 is upstream of the others.

### Parameters

The forces are calculated in the directions defined in Fig. 1, that is, x and y directions, whereas drag and lift forces are defined with reference to the incidence direction of the flow, that is, the drag force, $F_D$, is aligned with the flow direction and the lift force, $F_L$, is in the transverse direction. In the 0 degree incidence, the force in the x-direction, $F_x$, coincides with the drag load, $F_D$, whereas the force in the y-direction, $F_y$ coincides with the lift force, $F_L$. Conversely, for the 45 degrees incidence, the following rotation is done to obtain drag and lift forces from x and y forces:

$$\begin{bmatrix} F_L \\ F_D \end{bmatrix} = \begin{bmatrix} \cos(\theta) & \sin(\theta) \\ -\sin(\theta) & \cos(\theta) \end{bmatrix} \begin{bmatrix} F_x \\ F_y \end{bmatrix}. \quad (1)$$

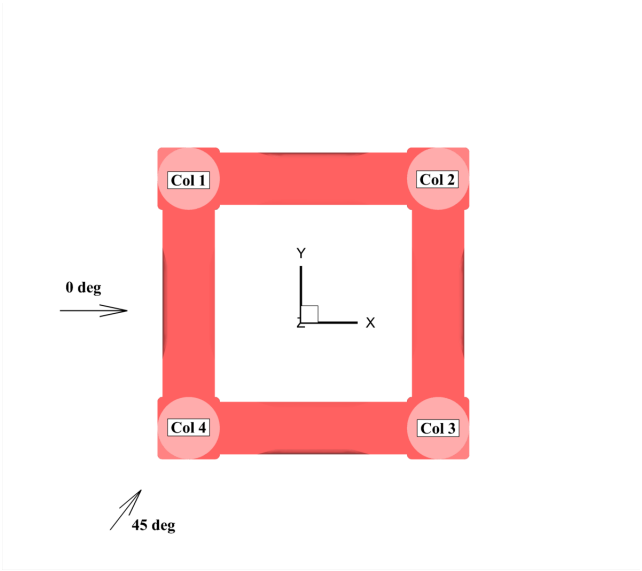


**FIGURE 1**. Incidence convention adopted for the calculations showed herein.

The same rotation is carried out when converting x and y motions into in-line and transverse motions.

The force in the x-direction is calculated within the CFD simulation as:

$$\mathbf{F_x} = \mathbf{e_x} \oint (-P\mathbf{n} + \nu(\nabla\mathbf{v} + \nabla\mathbf{v}^T)\mathbf{n})ds, \tag{2}$$

where $\mathbf{n}$ is the outward-pointing vector normal to the body surface; $e_x$ is a unit-vector aligned with the x-axis. The transverse force is defined as:

$$\mathbf{F_y} = \mathbf{e_y} \oint (-P\mathbf{n} + \nu(\nabla\mathbf{v} + \nabla\mathbf{v}^T)\mathbf{n})ds. \tag{3}$$

The drag coefficient is defined as:

$$C_D = F_D / \frac{1}{2}\rho A_{ref} V_\infty^2, \tag{4}$$

whereas the lift coefficient is defined as:

$$C_L = F_L / \frac{1}{2}\rho A_{ref} V_\infty^2. \tag{5}$$

The vorticity is calculated as:

$$\omega = \nabla \times \mathbf{v}. \tag{6}$$

The reduced velocity is calculated as:

$$V_R = \frac{V_\infty T_n}{D}, \tag{7}$$

in which $T_n$ is the natural transverse period and $D$ is the column diameter.

The nominal motion amplitudes are defined as:

$$(A/D)_{nom} = \sqrt{2}\frac{\sigma_A}{D}, \tag{8}$$

in which $\sigma_A$ is the standard deviation of the amplitude trace. The angles are defined in a similar manner. The nominal yaw values are written as:

$$(\phi)_{nom} = \sqrt{2}\sigma_\phi, \tag{9}$$

in which $\sigma_\phi$ is the standard deviation of the yaw angle time trace.

The yaw mass moment of inertia is defined as:

$$I_{yaw} = m r_z^2, \tag{10}$$

in which $m$ is the platform structural mass and $r_z$ is its radius of gyration in z-direction.

Important parameters can also be extracted from the loads and resulting vortex-induced motions, namely the parts of the lift force in phase with velocity and with acceleration of the moving platform (or the related concepts of damping and added mass, respectively). While their formulation is reasonably straightforward for the case of sinusoidally imposed motions due to a single imposed motion frequency and amplitude (as in the widely studied case of one cylinder, e.g. [8] among others), these ideas have to be carefully interpreted for the case of free motions, especially for a structure of more complex geometry, as in the present case. Furthermore, an essential issue pointed out by [8] is that this analysis is predicated on "(...) the assumption that the frequency and the amplitude of the oscillations remain constant" and "(...) oddly enough, this is more so for the forced oscillations than for the free oscillations". Moreover, as noted by [9], "the time functions of the lift, drag and amplitude look like sine functions, which are randomly modulated in amplitude and frequency. The instantaneous total force acting on the cylinder is then the result of the more or less cooperative behavior of these individual subsystems, which differ slightly from each other in frequency and amplitude". This means that the assumptions above render the problem more palatable, but also inspires additional care with taking conclusions from the analysis.

As mentioned above, in the case with imposed motions the parts in phase with acceleration and velocity are derived based

on the phase $\phi$ between the motion, $y_0 \sin(\omega t)$ and the lift force, $F_L = F_{L0} \sin(\omega t + \phi)$. In the present case, the motion is not defined previously, therefore an alternative method based on a frequency domain analysis is used:

$$\frac{\mathbf{F}(F_L)}{\mathbf{F}(y)} = m a_y \omega^2 - i c_{vy} \omega, \tag{11}$$

in which $\mathbf{F}(\cdot)$ denotes the Fourier Transform of a time signal, $ma_y$ is the added mass in the y-direction, $c_{vy}$ is the hydrodynamic damping value in the y-direction, $\omega$ is the frequency and $i$ is the imaginary number. The added mass coefficient is calculated as

$$Ca = m a_y / m_{disp}, \tag{12}$$

in which $m_{disp}$ is the displaced mass of the platform. Finally, the damping values can be given as factors of the critical damping value of linear system equation as follows:

$$\zeta = \frac{c_{vy}}{2 M_{Total} \omega_n}, \tag{13}$$

in which $M_{Total}$ is the total platform mass and $\omega_n$ is the natural frequency in the direction transverse to the flow. The added mass and damping are frequency-dependent, therefore the values presented herein correspond to the dominant motion frequency for each case (which disregards higher order components, inline with the initial assumptions). Phase angles can alternatively be calculated by means of Hilbert Transform $\mathbf{H}(\cdot)$, from which instantaneous amplitude and phase signals are obtained. One can thus obtain phase differences between different traces by subtracting the phase signals from their Hilbert Transform traces. The instantaneous frequency is obtained from time differentiation of the phase signal.

## DETAILS OF THE MODEL TESTS

The model tests were conducted to study the Vortex-Induced Motions (VIM) phenomenon of deep-draft Semi-Submersible (SS) platforms in a towing tank of 3.5m in depth, 6.6m in width and 280.0m in length. The circular column platform model had scale of 1:100 based on the typical geometry of a semisubmersible with four columns and four pontoons in closed configuration, see Fig. 2. The model was elastically mounted by means of a set of linear springs, which provide low structural damping. The range of towing velocities in the reduced velocity was 4 up to 25 covered Reynolds numbers from 7,000 to 80,000. For more details of the model tests, see [6].

**FIGURE 2**. Circular column model scale hull used in the model tests and calculations.

## DETAILS OF SETUP AND CALCULATIONS

### CFD Solver ReFRESCO

ReFRESCO [5] is a viscous-flow CFD code that solves multiphase (unsteady) incompressible flows using the Navier-Stokes equations, complemented with turbulence models, cavitation models and volume-fraction transport equations for different phases. The equations are discretised using a finite-volume approach with cell-centered collocated variables, in conservation form and a pressure-correction equation based on the SIMPLE algorithm is used to ensure mass conservation. Time integration is performed implicitly with first or second-order backward schemes. At each implicit time step, the non-linear system for velocity and pressure is linearised with Picard's method and either a segregated or coupled approach is used. A segregated approach is always adopted for the solution of all other transport equations. The implementation is face-based, which permits grids with elements consisting of an arbitrary number of faces (hexahedrals, tetrahedrals, prisms, pyramids etc) and if needed h-refinement (hanging nodes). State-of-the-art CFD features such as moving, sliding and deforming grids, as well automatic grid refinement are also available. For turbulence modelling, RANS/URANS, SRS approaches can be used. The code is parallelised using MPI and subdomain decomposition, and runs on Linux workstations and HPC clusters.

### Calculations Settings

In the present calculations, the URANS conservation equations are formulated and solved in the so-called moving grid or arbitrary Eulerian-Lagrangian approach [10]:

$$\frac{\partial \rho (U_i - U_{gi})}{\partial x_i} = 0, \tag{14}$$

$$\frac{\partial \rho U_i}{\partial t} + \frac{\partial}{\partial x_j}(\rho U_i(U_j - U_{gj})) = \frac{\partial}{\partial x_j}\left[(\mu + \mu_t)\left(\frac{\partial U_i}{\partial x_j} + \frac{\partial U_j}{\partial x_i}\right)\right] - \frac{\partial}{\partial x_i}\left(P + \frac{2}{3}\rho k\right), \quad (15)$$

in which $U_{gi}$ is the grid velocity, written more generally as $U_{gi} = U_{0i} + \varepsilon_{ijk}\Omega_j x_k$. In this relation, $\varepsilon_{ijk}$ is the Levi-Civita symbol, $\Omega_j$ is the rotational velocity and $U_{0i}$ is the translation velocity of the moving reference frame attached to the rigid body.

Regarding turbulence modeling, the k-$\omega$ SST model of [11] has been applied. This model has been widely applied due to the good performance in adverse pressure gradients and is known not to be largely sensitive to far-field turbulence values.

The segregated solver is applied herein: matrices for momentum and pressure are solved separately, and coupled by using a method based on the SIMPLE algorithm. The momentum convection scheme was the (second-order) quadratic upwind interpolation for convective kinematics (QUICK) with flux limiters. For the SST convection scheme, first-order upwind discretization (UD1) is applied.

The momentum and turbulence equations were solved using the generalized minimal residual method (GMRES) and the pressure Poisson equation was solved using the conjugate gradient (CG) method. Matrix pre-conditioning was performed using the modified Jacobi technique and the extrapolation of all boundaries was zeroth order. More details on those methods can be found in a number of references, such as [12].

Three degrees-of-freedom motion is modeled by means of a mass-spring-damper system as:

$$[M]\{\ddot{\mathbf{r}}\} + [C]\{\dot{\mathbf{r}}\} + [K]\{\mathbf{r}\} = \{\mathbf{F_{hydro}}\}, \quad (16)$$

in which $[M]$, $[C]$ and $[K]$ are the mass/inertia, structural damping and stiffness matrices, respectively and $\{\mathbf{r}\} = \{x, y, \phi\}^T$. The mass/inertia matrix is defined as:

$$[M] = \begin{bmatrix} m & 0 & 0 \\ 0 & m & 0 \\ 0 & 0 & I_{yaw} \end{bmatrix}. \quad (17)$$

The mechanical damping matrix represents the energy dissipation of the mooring setup, being defined as:

$$[C] = \begin{bmatrix} c_1 & 0 & 0 \\ 0 & c_1 & 0 \\ 0 & 0 & c_2 \end{bmatrix}. \quad (18)$$

The stiffness matrix is defined analogously as:

$$[K] = \begin{bmatrix} k_1 & 0 & 0 \\ 0 & k_1 & 0 \\ 0 & 0 & k_2 \end{bmatrix}. \quad (19)$$

Equation 16 is non-linear because the hydrodynamic forces, $F_{hydro}$, keep a non-linear relation with $\dot{\mathbf{r}}$, which evidently cannot be explicitly derived as they are obtained through the solution of the Navier-Stokes equations.

The information exchanged between the fluid and the solid domains basically consist of the loads exerted on the floater by the fluid and on the body velocity, fed back into the fluid domain equations iteratively upon solution of the problem.

In the present work, a strongly coupled scheme is applied as in [10]. The strongly coupled scheme used here is based on a second-order predictor-corrector scheme, in which the communication between flow solution and rigid body system is done at the time loop level with the predictor and at the outer loop level with the corrector. This scheme includes the flow field solution at time level $n+1$ in the prediction of the motion at the level $n+1$, which is the reason why it is also implicit for the fluid solver and therefore, strongly coupled. In the calculations showed herein, the corrector loops are calculated at each 5-10 outer loops with a $10^{-6}$ error criteria for the dynamic equations.

## Dynamic System Setup

The model scale adopted is 1:100 (Froude scaling) in both model tests and calculations showed herein. The dynamic setup has been replicated from the model tests carried out at the University of São Paulo to the present calculations. The main particulars and dynamic properties are defined below following the specifications of the USP model tests [6].

## Calculational Domain

The calculation domain used in the calculations showed herein are presented in Fig. 3. The farfield boundary has been set at a distance of 8L (thus nearly double of that in the model tests), in which L is the beam of the platform and the bottom boundary has been set at a distance of 7L from the top boundary.

## Geometry and Grids

The platform geometry and surface mesh used in the calculations is depicted in Fig. 4. The details of the pontoons and sharp edges at the base of the columns make the grid generation more difficult, requiring fine discretization to preserve the geometry and correctly calculate the flow in those areas. Figure 5 presents the grid layout at the water plane showing the refinement box

**TABLE 1**. Main particulars and dynamic properties used in the CFD calculations.

| Property | Unit | Value |
|---|---|---|
| Length ($L$) | m | 0.76 |
| Column Diameter ($D$) | m | 0.15 |
| Center to Center | m | 0.61 |
| Width of Pontoons | m | 0.13 |
| Draft ($T$) | m | 0.34 |
| Radius of Gyration | m | 0.49 |
| Mass ($m$) | $kg$ | 45.12 |
| Inertia ($I_{yaw}$) | $kgm^2$ | 6.85 |
| Linear stiffness ($k_1$) | $N/m$ | 23.45 |
| Rotational stiffness ($k_2$) | $N/rad$ | 18.0 |
| Linear struct. damping ($c_1$) | $kg/s$ | 0.01 |
| Rotational struct. damping ($c_2$) | $kgm^2/s$ | 0.01 |

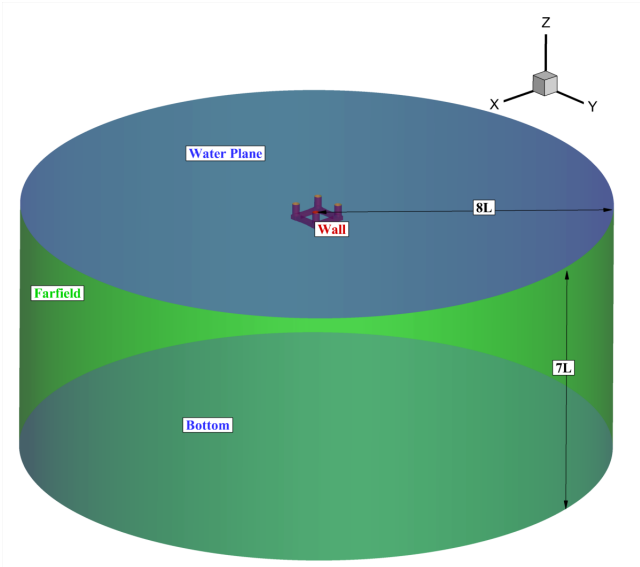


**FIGURE 3**. Calculation domain used in the computations.

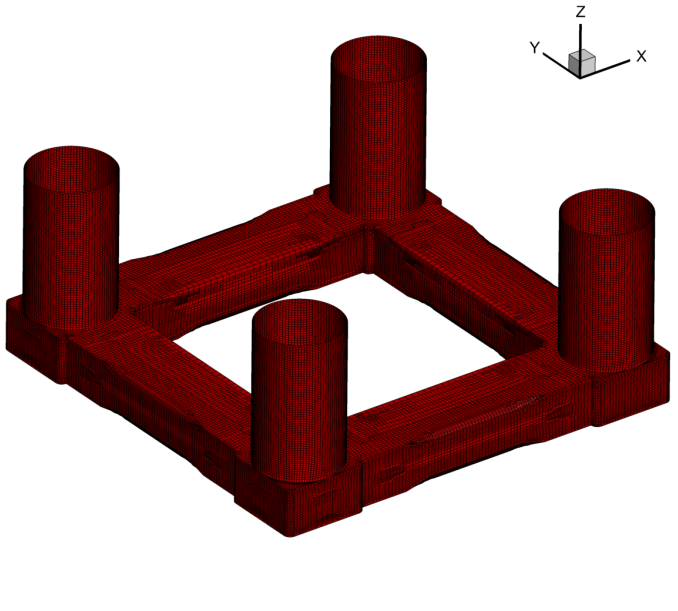


**FIGURE 4**. Details of the geometry of the platform used in the calculations.

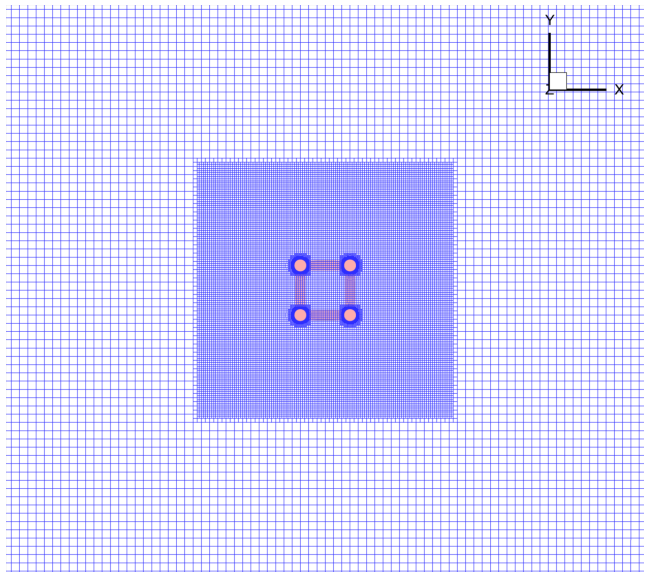


**FIGURE 5**. Details of the refinement box around the hull.

in the center of the domain to be able to capture the near wake region where the vortices shed from the columns are located.

The near wall refinement ensures that $y^+_{max} < 1.0$ at the cells nearest to the wall, a condition necessary to correctly calculate the velocity and pressure distribution near the wall without the need of using wall functions. Moreover, the near wall refinement stretched outwards with stretching ratio of 1.3.

A sensitivity analysis has been done with three different grids for reduced velocity $V_R = 7.0$ and incidences of 0 and 45 degrees. The intermediate grid has been found to be a good balance between processing time and accuracy, as the variations of results to the finest one are very small, as shall be seen below. Table 2 shows the grids used in the sensitivity analysis, together with the maximum and average values for $y^+$ at the cells adjacent to the wall. Values of $y^+$ nearly or lower than 1 have been

observed in all reduced velocities.

## Initial and Boundary Conditions

With regards to the boundary conditions, at the top and bottom boundaries a symmetry condition is enforced, in which the convective fluxes of all quantities are zero on that boundary, as well as the normal gradients of the scalar quantities and the velocity components parallel to the symmetry plane. That modeling choice is associated with an hypothesis of negligible effect of the free surface on the VIM of the platform.

The farfield boundary is comprised of an inlet boundary of ca. 33% of the circumference length and a pressure condition at the remaining portion is enforced. At the inlet, an inflow condition is applied, in which the velocity and turbulent quantities are specified with Dirichlet boundary condition, whereas pressure is extrapolated from the interior solution (zeroth-order extrapolation); outside of the inflow boundary the pressure condition applies, which is similar to the symmetry condition, except for the Dirichlet condition for pressure (i.e. a constant value is enforced). At the platform surface, a non-slip condition applies.

For initial conditions, uniform laminar velocity, pressure and eddy viscosity fields are imposed in the entire field, in which the velocity magnitudes correspond to each reduced velocity.

## Iterative Convergence

The iterative convergence criteria has been set based on the RMS norm of the normalized residuals; in particular, $L_2 \leq 10^{-4}$ is pursued for all equations within each time step. The $L_\infty$ norm of the residuals have been monitored and it is normally one to two orders of magnitude larger than $L_2$. Since the former is a local quantity it is common to notice few locations at the flow where $L_\infty$ is of the order $10^{-2}$ but not important to the flow overall. Conversely, the $L_2$ norm measures a residual distribution in the field reaching a more practical evaluation of the iterative convergence. In the iterative criteria for the dynamic equations, the error criteria is set to $10^{-6}$ in all time steps.

## Sensitivity Analysis

A grid and time step sensitivity analysis has been carried out in order to determine the grid and time steps that would be used in the calculations for all the reduced velocities. As commented above, this analysis has been carried out for $V_R = 7.0$ both for 0 and 45 degrees of incidence, with three grids and three time steps. Figures 6 and 7 show these results focusing on the transverse motion. It is noticed that there is a large variation between the coarsest grid and the other ones. There are small variations of the forces and motions from the intermediate to the finest grid.

Moreover, $T_{ref}/\Delta t > 400$ seems to be fine enough, as the variation of nominal transverse results are at most smaller than 4%. For these reasons, the calculations done with the other reduced velocities as well as the decay calculations were carried out using the intermediate grid (6,347,134 cells) and time steps such that $T_{ref}/\Delta t = 427$, providing results that are converged and cost-effective in terms of discretization.

**TABLE 2**. Grids used for the sensitivity analysis done for $V_R = 7.0$ with $T_{ref}/\Delta T = 427$ for 0 and 45 degrees incidences.

| Grid | Num. of cells | $y^+_{max}$ - 0 deg | $y^+_{avg}$ - 0 deg | $y^+_{max}$ - 45 deg | $y^+_{avg}$ - 45 deg |
|---|---|---|---|---|---|
| 1 | 4,553,794 | 0.32 | 0.06 | 0.20 | 0.01 |
| 2 | 6,347,134 | 0.53 | 0.02 | 0.41 | 0.01 |
| 3 | 7,980,182 | 0.60 | 0.02 | 0.29 | 0.01 |

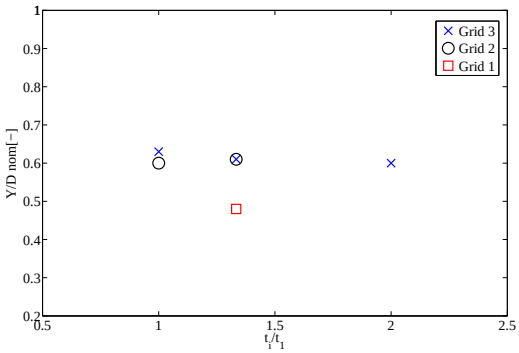


**FIGURE 6**. Sensitivity of the transverse motions to different grids and time steps for the case with 0 degree of incidence and $V_R = 7.0$. In this plot, $t_1$ is the finest time step used.

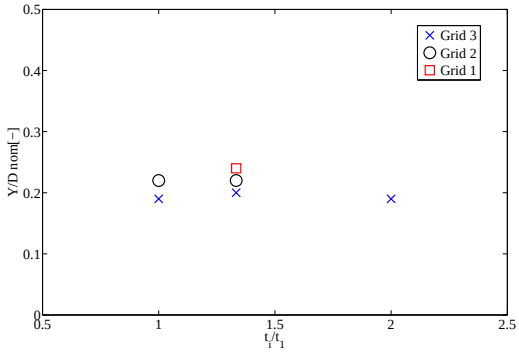


**FIGURE 7**. Sensitivity of the transverse motions to different grids and time steps for the case with 45 degrees of incidence and $V_R = 7.0$. In this plot, $t_1$ is the finest time step used.

## DECAY ANALYSIS

### Approach

Decay analyses have been done using the same setup as the VIM calculations for the transverse motion direction in 0 and 45 degrees incidences and for the yaw degree-of-freedom. For these cases, a very low inflow velocity is imposed to improve convergence: $V = 0.0001m/s$, which corresponds to 0.1% of the inflow velocity for $V_R = 7.0$. The results presented herein include the natural periods, linear, quadratic and total damping according to the procedure outlined in [13]. The decay is modelled by the following equation:

$$m_i\ddot{r}_i + c\dot{r}_i + \frac{8b_2}{3\pi}\omega_N r_k r_i + kr_i = 0, \tag{20}$$

in which $b_2$ is the quadratic damping term, $\omega_N$ is the natural frequency of the i-th degree-of-freedom and $r_k$ is the intial amplitude of the analyzed cycle. The hydrodynamic damping coefficient is defined as:

$$\zeta_i = \frac{c_i}{2(M_{total}\omega_N)}. \tag{21}$$

The total damping is defined as:

$$c_{i,total} = c_i + \frac{8b_2}{3\pi}\omega_N r_k. \tag{22}$$

In the sway decay 0 degree incidence, the platform was given an offset of $Y/D = 0.25$ and let to oscillate freely; for the 45 degrees decay, the platform was offset by $\sqrt{(X/D)^2 + (Y/D)^2} = 0.25$; for the yaw decay, the initial angle was set as 5 degrees.

### Results

Table 3 show the natural periods and damping values for the CFD calculations in comparison with the USP model tests. For the decay in transverse direction in 0 and 45 degrees, the differences in the natural periods reach ca. 2.9% in both cases, whereas for the yaw, a difference of 8.5% is observed.

## VIM ANALYSIS

### Approach

CFD calculations have been carried out for both 0 and 45 degrees incidence. For the cases showed herein, the simulations started with the captive platform, with flow velocity corresponding to their reduced velocities. After the flow is established (which is seen by steady-state forces), the platform is "released" and motions take place freely in 3 DOF.

**TABLE 3**. Natural periods, linear, quadratic and total damping values for the calculations compared to the experimental values obtained in the USP model tests.

| Case | Period(s) | $\zeta$(linear) |
|---|---|---|
| Sway 0 deg CFD | 11.58 | 2.60% |
| Sway 0 deg Exp. | 11.93 | 1.50% |
| Y 45 deg CFD | 11.57 | 1.40% |
| Y 45 deg Exp. | 11.93 | 1.30% |
| Yaw CFD | 4.92 | 0.90% |
| Yaw Exp. | 5.38 | 1.20% |

The maximum amplitudes in the experiments might be strongly influenced by any type of disturbance of the flow, which otherwise do not occur in the calculations. For that reason, the comparison of nominal values seems to be more consistent than using the maxima. We have tried to obtain at least ten cycles from the CFD runs, which usually led to three to four weeks of computation time in a High-Performance Computing cluster, normally using 100 cores (2.8GHz clock speed and 3GB of RAM per core).

### 0 degree Incidence

Figure 8 show respectively the nominal nondimensional amplitudes of $X$ and $Y$ motions from the CFD calculations compared to the model test results for 0 degrees incidence. A fair agreement is observed, although somewhat larger in the calculations. For $V_R = 5.0$, low amplitudes were observed in the CFD calculations due to undeveloped VIM response. It is possible that the pulley system induced reasonable mechanical damping levels, thus reducing the motion amplitudes.

A clear resonance behavior is observed for reduced velocities between $V_R = 7.0$ and $V_R = 10.0$, after which irregular forces and motions are observed. Interestingly, the behavior for 0 degree incidence is different from that observed in the square columns case [6], in that the amplitudes for the present case are much larger than the values for the square columns platform in 0 degrees. It is quite clear that the circular columns imposes distinct flow and response characteristics.

Figure 9 show the nominal yaw amplitudes, in which good agreement is observed between calculations and experiments. For $V_R = 12.0$, the calculated yaw amplitudes are smaller than in the model tests. Conversely, the transverse motion in the same reduced velocity is larger in the calculation compared to the model tests result, which indicates some energy transfer from one degree of freedom to the other in that reduced velocity.

Figure 10 shows the average drag coefficients of the calculations in comparison with the experiments. There is a fair agree-

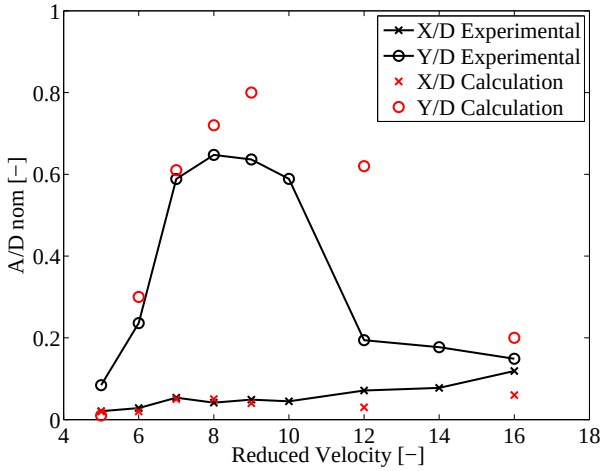


**FIGURE 8**. Nominal nondimensional $X$ and $Y$ amplitudes with 0 degree flow incidence.

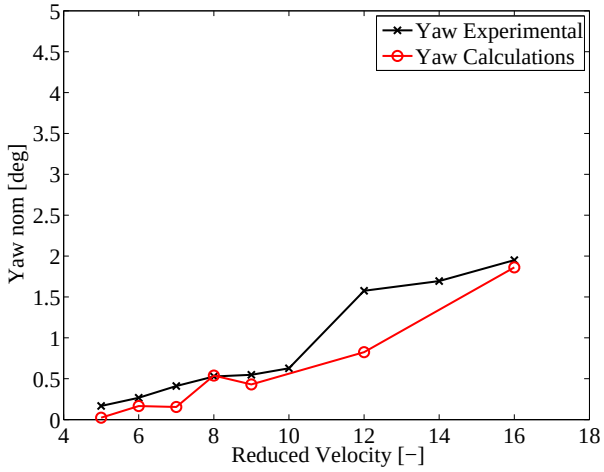


**FIGURE 9**. Nominal yaw amplitudes with 0 degree flow incidence.

ment in the trends and values, except for $U_R = 5.0$, in which the calculation displays a lower value, associated with lower motion amplitudes as noted above. It is quite clear that the vortex induced motions indeed amplify the mean drag in spite of low dynamic response in the in-line direction. That evidently would have an important effect on the mooring and riser systems.

Along similar lines, Fig. 11 shows the rms of the lift coefficients for the calculations and model test results, where once again the amplification of the force occurs at around $U_R = 7.0$. Close observation of the results shows that for, $V_R = 12.0$, despite low values of lift coefficient, the motion amplitude remains at a large value. That is mainly due to the observed phase lag between lift force and transverse motion in that reduced velocity, showed in Fig. 12. The time dependent phase remains at values near -108 degrees (the average value), so that the lift in phase with velocity is appreciable (it depends on the sine of the phase lag, $C_{LV} = C_{Lamp} sin\theta$). Furthermore, as it results in a negative value, it means that there is energy transfer from the fluid to the body ("negative damping"), which explains the large amplitude of motion. In the experiments, it has been noticed that the yaw amplitudes are somewhat larger than in the calculations (see Fig. 9), draining a part of the energy from the fluid. The response in the other degrees of freedom can also enhance the same behavior.

Along that discussion, Fig. 13 shows the hydrodynamic damping coefficients as a factor of the critical damping values. It is noticed that up to $U_R = 9.0$, these values are low and positive, which cause "positive damping" of the structure, and the motions are mainly determined by the high lift amplitudes, due to resonance. For higher reduced velocities, phase plays a larger role in regulating forces and motions. Figure 14 shows the total added mass coefficients for the calculations and model tests, in which there is fair agreement of the results, although higher values are found in the calculations. The added mass values relates to the total lift force in phase with acceleration. The decrease of the added mass coefficient in increasing reduced velocities means that the virtual mass "dragged" by the system is decreasing and the system is becoming "lighter". Therefore, lower lift values are able to displace the platform comparatively more than in the lower reduced velocities, until the the vortex-shedding frequency becomes larger than the sway natural frequency. From that point on, an amplification of yaw takes place.

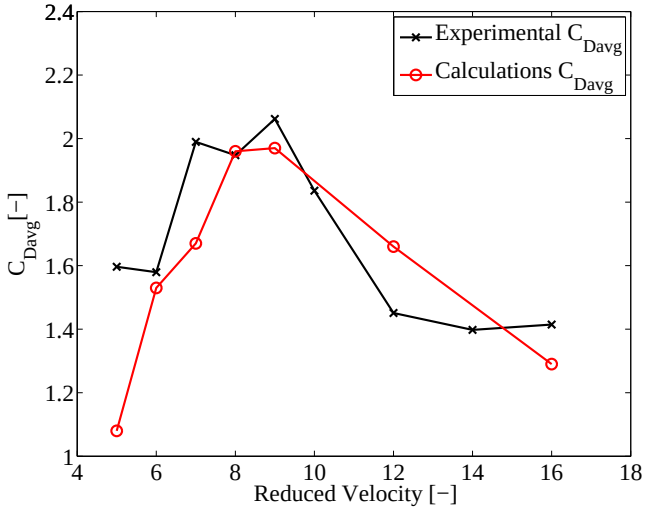


**FIGURE 10**. Average drag coefficients for the 0 degree flow incidence.

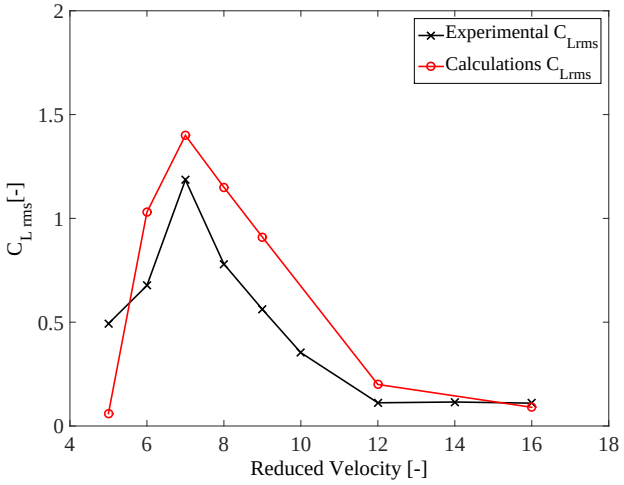


**FIGURE 11**. The rms of lift coefficients for 0 degree flow incidence.

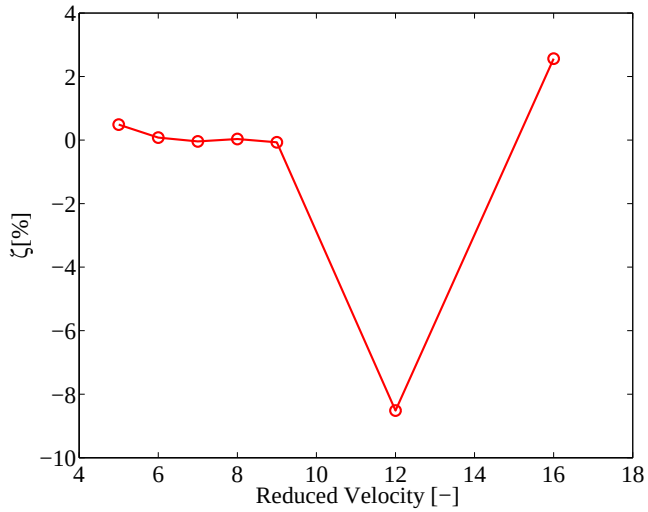


**FIGURE 13**. Hydrodynamic damping coefficients as a factor of critical damping for 0 degree flow incidence.

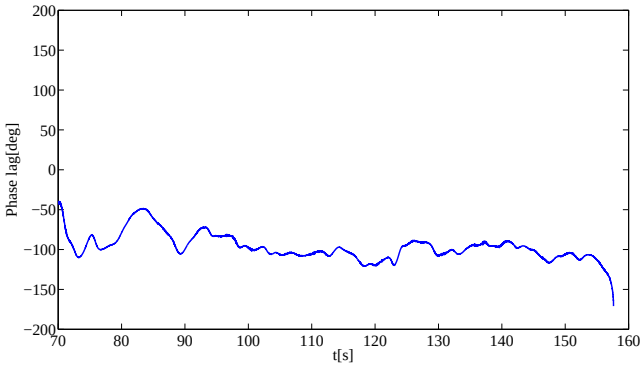


**FIGURE 12**. Time-dependent phase lag between the lift force and transverse motion for $V_R = 12.0$ and 0 degree incidence.

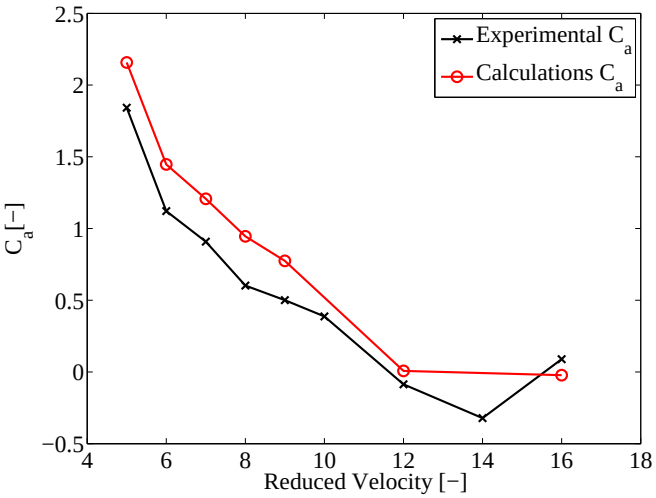


**FIGURE 14**. Added mass coefficients for the 0 degree flow incidence.

Figure 15 shows the $Y$ time signature, transverse loads on the four columns, pontoons and total loads and the columns and pontoons time dependent force phases with respect to the total forces calculated with the Hilbert Transform for $V_R = 7.0$. One notes that the loads on columns are nearly in phase with each other, justifying a strong net transverse force (in the middle frame) and large transverse motions. On the other hand, Fig. 16 shows the same plots for $V_R = 12.0$, in which there is large variability of the phase lag between columns the total force, indicating lack of synchronization (nearly constant phase lags between forces and total force indicate frequency synchronization and oscillation of the phase lag indicates that the dominant frequencies are different). It is also possible to notice small contribution of the forces on the columns to the total force. Conversely, the loads on the pontoons seem to be dominant and with constant phase lag with respect to the total force, indicating a stronger level of synchronization. That means that, at higher reduced velocities, the flow around the pontoon is contributing more to the net loads and motions than the columns.

Figure 17 show nondimensional z-vorticity and nondimensional eddy viscosity and slices of in the vertical direction at

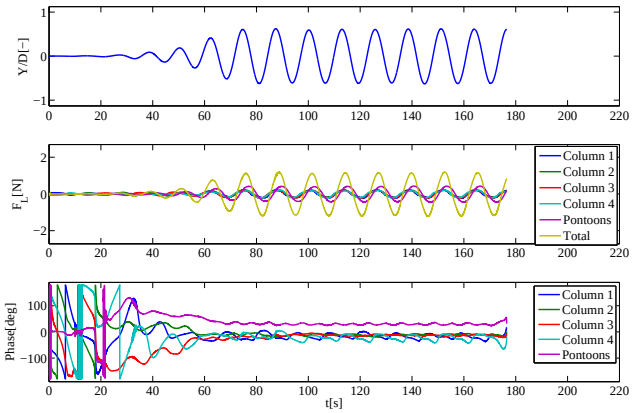


**FIGURE 15**. Plots showing the nondimensional transverse motion $(Y/D)$ on the top frame. Force traces of each column, pontoons and total force in the middle frame. Force phases with respect to the total force for columns and pontoons in the lower frame. Results for the 0 degrees incidence and $V_R = 7.0$

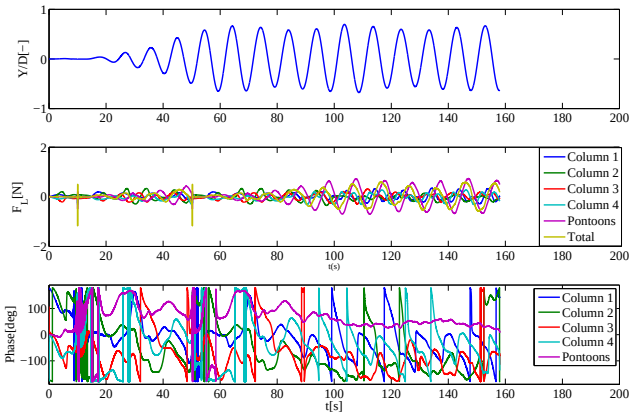


**FIGURE 16**. Plots showing the nondimensional transverse motion $(Y/D)$ on the top frame. Force traces of each column, pontoons and total force in the middle frame. Force phases with respect to the total force for columns and pontoons in the lower frame. Results for the 0 degrees incidence and $V_R = 12.0$

$z/T = 0.85$, measured from the keel up and at the maximum motion amplitude instant for $V_R = 7.0$. The wake is reasonably organized and the vortices shed from the columns are more coherent and nearly in phase with each other improving the total force. The wake of the upstream columns develops enough to form strong vortices that impact the downstream columns and determine their flow dynamics. A noticeable turbulent flow is observed downstream of the platform, but less intense between the upstream and downstream columns, marked by values $1.0 < \nu_t/\nu < 10.0$.

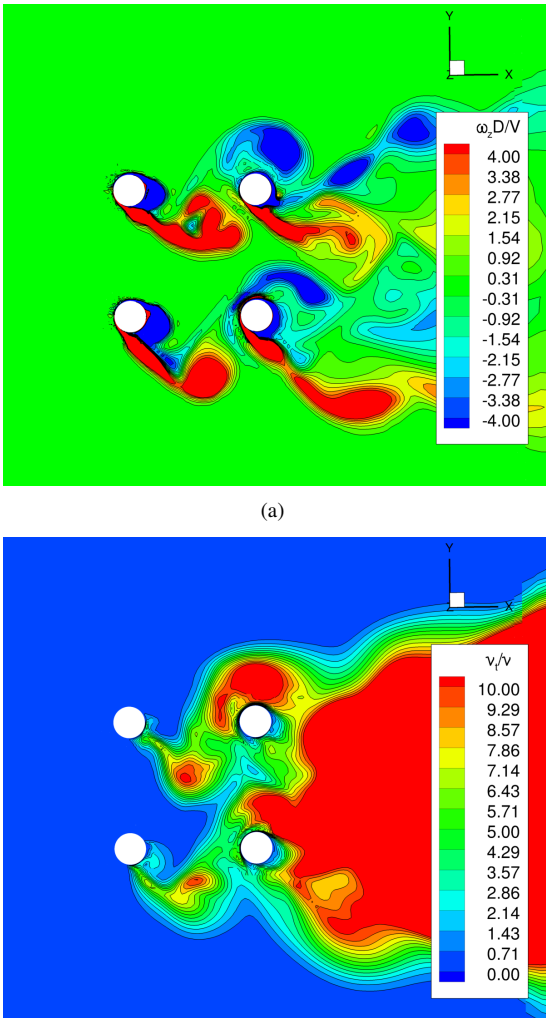


**FIGURE 17**. Plot of quantities at the vertical plane $z = 0.3m$ extracted at the instant of maximum transverse platform motion. Results for $V_R = 7.0$ and 0 degrees incidence. (a) Nondimensional vorticity in the vertical direction $\omega_z D/V$. (b) Nondimensional eddy viscosity.

## 45 degrees Incidence

Figure 18 show the nominal amplitudes of $X$ and $Y$ motions from the CFD calculations compared to the model test results for 45 degrees incidence. The agreement observed both for nominal and for maximum amplitudes is fair, as seen for 0 degrees incidence. It is known that the cylinder flow is one of the most challenging cases for CFD calculation and, for this case, there are

three exposed columns, thus making experimental results much more challenging to be captured. Fully turbulent flows and cases with several geometric details enable a more favorable situation from a modeling perspective. Further investigation on this issue is being carried out to determine wether the turbulence model and other modeling issues are relevant.

Figure 19 shows the nominal yaw amplitudes, in which good agreement is observed. Quite high amplitudes are observed for $U_R = 16.0$, as also seen in the transverse motion results. In that reduced velocity, both transverse motion and yaw dominant periods are near their respective natural periods, indicating some degree of motion synchronization, even for such high reduced velocity. It is quite evident, however, that those reduced velocities would result in very large full scale flow velocities, such that the practical consequences of that second response peak are possibly unimportant.

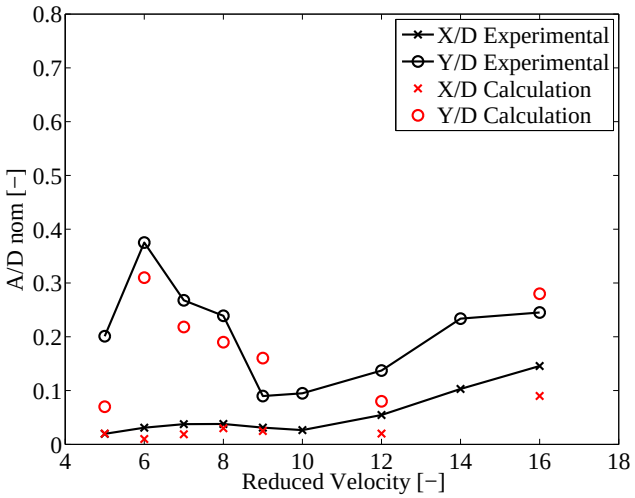


**FIGURE 18**. Nominal nondimensional $X$ and $Y$ amplitudes with 45 degree flow incidence.

Figure 20 shows the average drag coefficients, in which an amplification in the resonance range is observed, although with a peak at $V_R = 6.0$ in the calculations and at $V_R = 7.0$ in the model tests. For reduced velocities larger than $V_R = 10.0$, the drag increases again due to a new amplitude peak, now both in the transverse direction and yaw degree of freedom. The rms of lift coefficients are presented in Fig. 21, in which there is a fair agreement, except for $V_R < 7.0$, which also corresponds to a poor agreement in terms of motions.

Figures 22 and 23 show the damping and added mass coefficients, respectively. Regarding the damping coefficient, similar behavior to the 0 degree incidence is observed, with small positive damping in low reduced velocities and larger absolute values in larger reduced velocities, mainly due to the phase between forces and motions. For $U_R = 16.0$, a large negative damping is seen causing an increase of the motions due to energy transfer from the fluid to the body. Regarding the added mass coefficients, the same trends observed the the 0 degree incidence are seen again: the virtual mass decreases with increasing reduced velocities so that the system becomes "lighter" and thus requiring lower lift coefficients for a relatively large motion.

Figure 24 and 25 show the $Y$ time signature; transverse loads on the four columns, pontoons and total loads; and the columns and pontoons time dependent force phases with respect to the

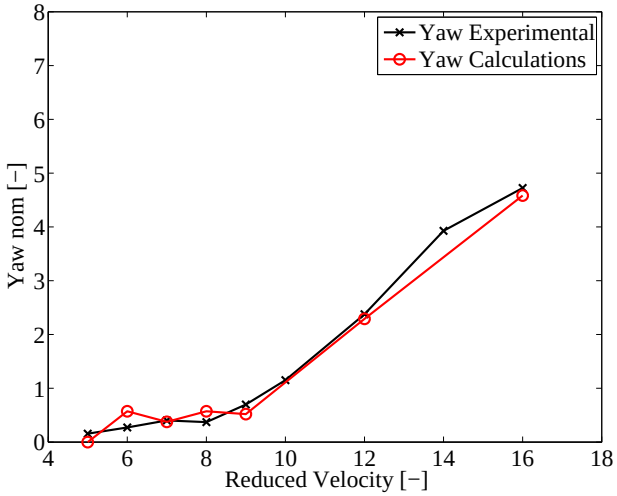


**FIGURE 19**. Nominal yaw amplitudes with 45 degree flow incidence.

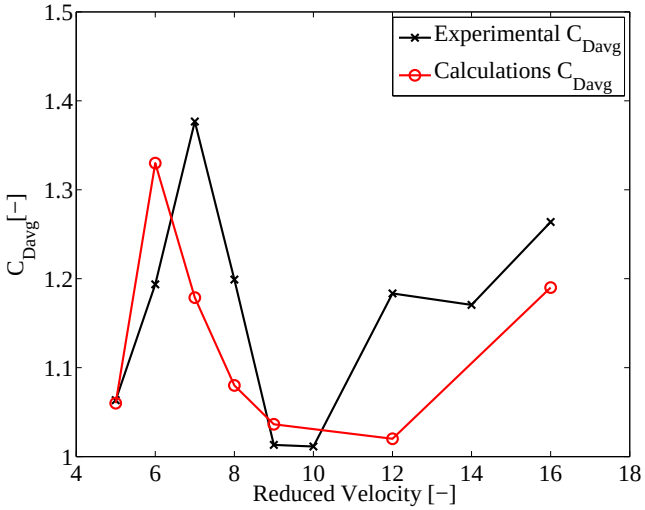


**FIGURE 20**. Average drag coefficients for the 45 degree flow incidence.

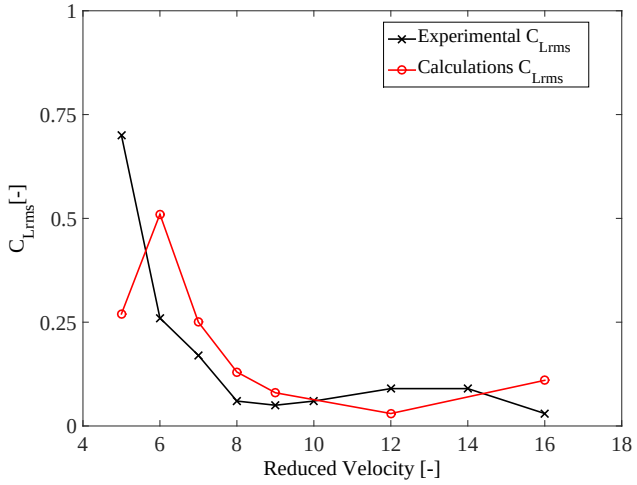


**FIGURE 21**. The rms of lift coefficients for 45 degree flow incidence.

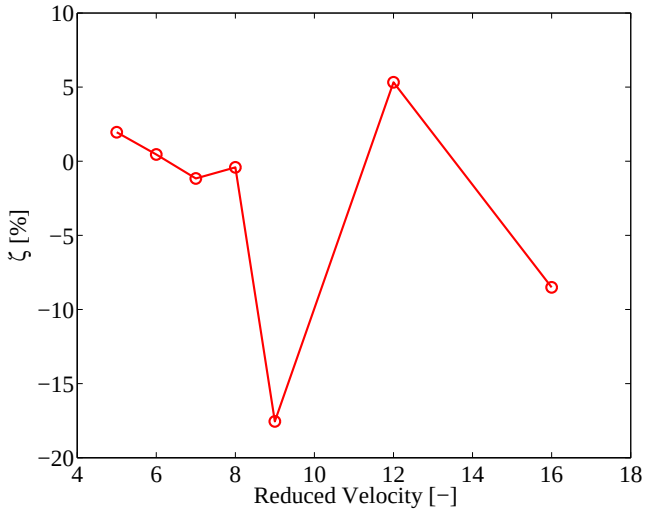


**FIGURE 22**. Hydrodynamic damping coefficients as a factor of critical damping for 45 degree flow incidence.

total forces calculated with the Hilbert Transform, respectively for $V_R = 6.0$ and $V_R = 7.0$ with 45 degrees of incidence. In both cases, one notes that the lift forces on columns 1 and 3 are nearly in phase with each other and the forces on column 2 (downstream column) and the pontoons are in phase with each other. As seen for the 0 degree incidence, within the locked region, there is synchronization of the forces on columns and pontoons and the in-phase forces causing large net force. That, in turn, is able to cause appreciable motions in that range. For larger reduced velocities, synchronization of the columns cease to take place, but the pontoons display steady force, largely contributing to the total force. In this range, the phase between total force and motion is quite important, determining wether amplification or damping of the motions take place.

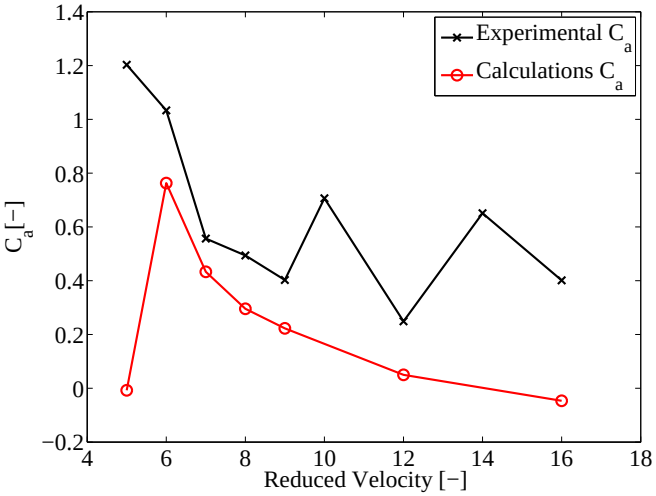


**FIGURE 23**. Added mass coefficients for the 0 degree flow incidence.

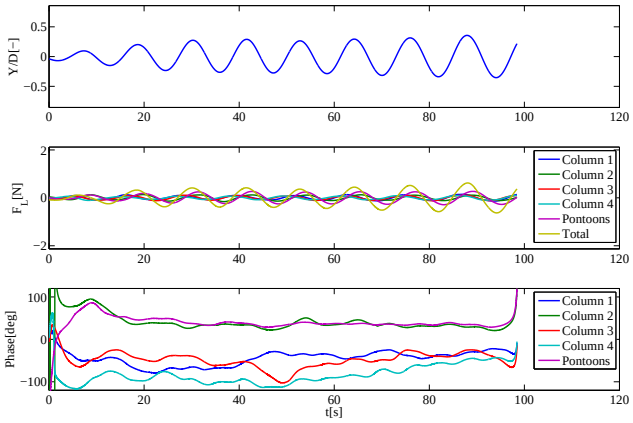


**FIGURE 24**. Plots showing the nondimensional transverse motion ($Y/D$) on the top frame. Force traces of each column, pontoons and total force in the middle frame. Force phases with respect to the total force for columns and pontoons in the lower frame. Results for the 45 degrees incidence and $V_R = 6.0$

As done above, Fig. 26 show nondimensional z-vorticity and nondimensional eddy viscosity and slices of in the vertical direction at $z/T = 0.85$, measured from the keel up and at the maximum motion amplitude instant. The same observation is done

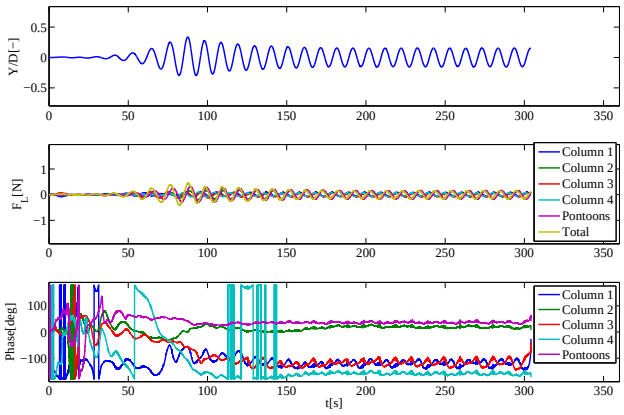


**FIGURE 25**. Plots showing the nondimensional transverse motion $(Y/D)$ on the top frame. Force traces of each column, pontoons and total force in the middle frame. Force phases with respect to the total force for columns and pontoons in the lower frame. Results for the 45 degrees incidence and $V_R = 7.0$

for the 0 degree incidence: the wake is reasonably organized and the vortices shed from the columns are coherent as one moves up from the keel. The vortices shed from columns 1 and 3 are indeed synchronized and in phase. The distance from column 4 to column 2 is larger thus enabling the formation of a well defined and independent wake from column 4.

## ON THE BEHAVIOR OF HYDRODYNAMIC DAMPING

There has been some debate regarding the meaning of positive and negative hydrodynamic damping coefficients from the results showed above. It is firstly important to address a definition issue in that regard: while treating the parts of the lift force in phase with velocity and acceleration it is normal to consider these components on the right-hand side of a dynamic equation such as Eq. 16, with amplitudes related to their contribution to the total force. It is also possible to have those force amplitudes manipulated to become components on the left-hand side being related to the mechanical parameters of the dynamic system and to name them damping and added mass coefficients. Consequently, when observing a positive contribution (positive amplitude or coefficient) of the lift force in phase with velocity (on the right-hand side), there would be energy being transferred from the fluid to the body and the work done by the fluid is positive over a cycle. In turn, the same behavior would be observed if one calculated the force component in phase with velocity treating it as damping (on the left-hand side), with the signal would be opposite: hydrodynamic damping would be negative with energy still being transferred from the fluid to the body. The opposite also holds, meaning that if the force component in phase were negative (or

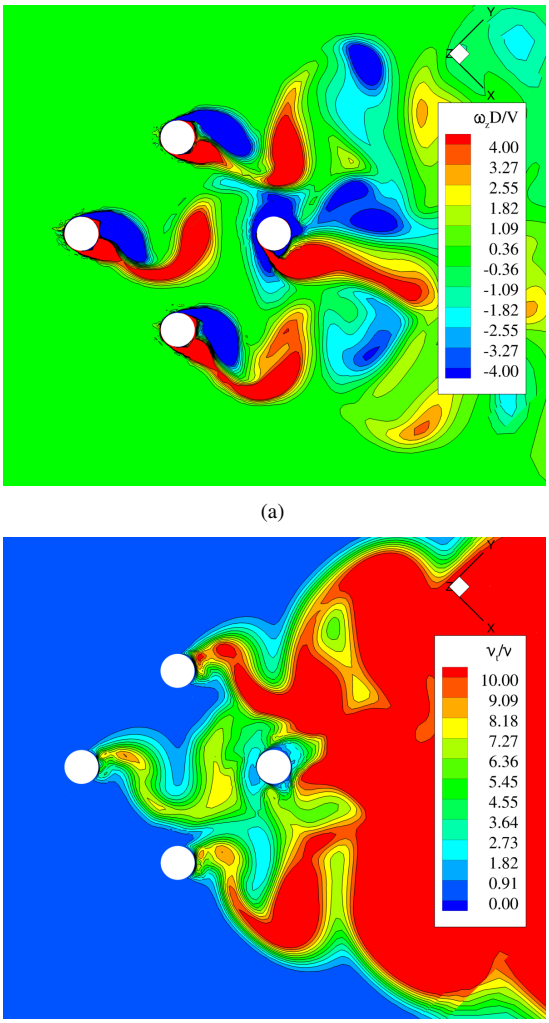


**FIGURE 26**. Plot of quantities at the vertical plane $z = 0.3m$ extracted at the instant of maximum transverse platform motion. Results for $V_R = 7.0$ and 45 degrees incidence. (a) Nondimensional vorticity in the vertical direction $\omega_z D/V$. (b) Nondimensional eddy viscosity.

damping, positive) the fluid would then be removing energy from the body system and the motions would be damped.

Several researchers have reported on this type of analysis for the imposed motions of a single round cylinder, e.g. [8, 10, 14], but not fro free motions. It has been noted that the connection between forced and free motion with regards to the phase between motion and force is not straightforward. In free motions, frequencies and amplitudes of both motions and forces can be irregular and modulated and might contain energetic harmonics, meaning that the definition of one phase value for the complete time trace is associated with strong assumptions. As discussed by [10, 14] for the cylinder case, those assumptions are reason-

able and the results are that for nondimensional motion amplitudes below 0.5 and in resonance, damping can be positive (energy is drawn from the system by the fluid to limit the motions), whereas out of resonance, damping can become negative (positive energy from the fluid to the body) in order to increase the motions (self-excitation).

Accepting possible limitations of the underlying assumptions for the present case, negative and positive damping coefficients were observed in the calculations. According to the ideas above, positive hydrodynamic damping was noted for peak amplitude motions, meaning positive energy transferred from the body to the flow limiting motions (self-limitation). Conversely, negative damping (positive energy transfer from the fluid to the body) was usually noted out of the resonance range in cases with moderate motions, resembling the self-excitation feature of vortex-induced vibrations.

## CONCLUSIONS

This paper presented the CFD calculations pertaining model scale VIM for a multi-column floater. In particular, the VIM of a floater with circular columns has been investigated for 0 and 45 degrees incidence over a range of reduced velocities. A sensitivity analysis of grid and time steps has been carried out to determine the configuration which allows a favorable balance of accuracy and computation requirement. A grid with 6,347,134 cells and 427 calculation steps in each hydrodynamic time step have been considered appropriate.

Decay tests in the transverse direction to the flow with 0 and 45 setups and yaw decay tests have been calculated and compared to model tests presenting up to ca. 8% relative differences in natural periods. This difference could be attributed to the combination of differences in the damping and added inertia between calculations and model tests. The damping values obtained be means of standard techniques show results which are in fair agreement with the model tests.

Regarding the 0 degree incidence, the VIM calculations for reduced velocities 5.0, 6.0, 7.0, 8.0, 9.0, 12.0 and 16.0 have been carried out, showing a fair agreement of transverse (sway), inline (surge) and yaw amplitudes as well as oscillation periods, except for $V_R = 5.0$ and $V_R = 12.0$. For these reduced velocities in the experiments, the flow is less organized and as the mass ratio of the structure is low (for a floater, without considering riser and mooring systems, $m^* = 1.0$), the system is more susceptible to the flow disturbances which damp the motion. In the calculations, these random perturbations and small scale disturbances are very small or absent. Moreover, it is important to notice that when forces or motions are small in amplitudes, small absolute differences can represent large relative deviations. It is also pointed out that marginal improvements can be achieved by modeling the other rotational degrees of freedom, as small amplitude roll motions have been observed in the experiments (ca. 1-1.5 deg). The forces on the columns showed to be nearly in phase with each other causing large net transverse forces and thus motions. For the larger reduced velocities, the flow around the columns cease to be synchronized.

For the 45 degrees incidence, the same range of calculations as the 0 degree case are carried out. Good agreement has been found for the motion amplitudes with some discrepancy for $V_R = 5.0$ and $V_R = 12.0$, although the comparison for these reduced velocities remains with the largest relative differences. Regarding oscillation periods, the comparison is fair, in that some of the predominant periods found in the calculations and experiments are different. Nevertheless, it is important to notice that this issue mainly occurs with small energy motions, in which comparison becomes more troublesome. It has been found that the upstream column seems to shed vortices with different phase from the others, whereas the side column forces are in phase with each other and the downstream column force is in phase with the pontoons force. This resulted in smaller net transverse forces compared to the 0 degree incidence, as also observed in [15].

It has been pointed out that, within the lock-in range, the synchronization of the forces on columns and pontoons and the in-phase forces cause large net transverse forces. Appreciable motions thus result. For larger reduced velocities, synchronization of the columns cease to take place, but the pontoons display synchronized force, largely contributing to the total force. In this range, the phase between total force and motion is quite important, determining wether amplification or damping of the motions take place. Positive damping determines energy transfer from the fluid to the body, causing the amplification of the motion. Further investigation on the energy issues is being conducted also for the model tests in order to verify those issues.

## ACKNOWLEDGMENT

This study was carried out within VIM JIP, which is run by the partnership between MARIN and USP, and for whose participants the authors are grateful. The participants of the VIM JIP are: MARIN, USP, Granherne, KBR, GVA, SBM Offshore, Petrobras, Aker Solutions and ConocoPhilips.

## REFERENCES

[1] DNV, 2008. Offshore standard - position mooring. Tech. Rep. E301, Det Norske Veritas.

[2] Ma, W., Wu, G., Thompson, H., Prislin, I., , and S., M., 2015. "Vortex induced motions of a column stabilized floater". *Proceedings of the International D.O.T. Conference Houston, USA*.

[3] Koop, A., Wilde, J., Fujarra, A., Rijken, O., Linder, S., Lenblad, J., Haug, N., and Phadke, A., 2016. "Investigation on reasons for possible differences between VIM re-

sponse in the field and in model tests". *In Proceedings of OMAE2016, June 19June 24, Busan, Korea*.

[4] Kim, S., Spernjak, D., Holmes, S., Vinayan, V., and Antony, A., 2015. "Vortex-induced motion of floating structures: Cfd sensitivity considerations of turbulence model and mesh refinement". *In Proceedings of OMAE2015, May 31June 5, St. John's, Newfoundland, Canada*.

[5] REFRESCO, 2015. Refresco website. www.refresco.org. Accessed: 2015-05-17.

[6] Gonçalves, R., Fujarra, A., Rosetti, G., Kogishi, A., and Koop, A., 2015. "Effects of column designs on the VIM response of deep-draft semi-submersible platforms". In Proceedings of the 25th International Offshore and Polar Engineering. Kona, Hawaii, USA.

[7] Koop, A., Rijken, O., Vaz, G., and Maximiano, A. Rosetti, G., 2015. "Cfd investigation on scale and damping effects for vortex-induced motions of a semi-submersible floater". *In Proceedings of OMAE2015, May 31June 5, St. John's, Newfoundland, Canada*.

[8] Sarpkaya, T., 2004. "A critical review of the intrinsic nature of vortex-induced vibrations". *Journal of Fluids and Structures,* ***19***, pp. 389–447.

[9] Schewe, G., 1983. "On the force fluctuations acting on a circular cylinder in cross-flow from subcritical up to transcritical reynolds numbers". *Journal of Fluid Mechanics,* ***133***, pp. 265–285.

[10] Rosetti, G., 2015. "Improvements in the numerical modeling of turbulence and fluid-structure interaction for the vortex-induced vibrations of a rigid cylinder". PhD thesis, University of São Paulo.

[11] Menter, F., Kuntz, M., and Langtry, R., 2003. "Ten years of industrial experience with the sst turbulence model". *Turbulence, Heat and Mass Transfer 4*, pp. 625–632.

[12] Balay, S., Abhyankar, S., Adams, M. F.and Brown, J., Brune, P., Buschelman, K., Eijkhout, V., Gropp, W. D., Kaushik, D., Knepley, M. G., McInnes, L. C., Rupp, K., Smith, B. F., and Zhang, H., 2013. PETSc users manual. Tech. Rep. ANL-95/11 - Revision 3.4, Argonne National Laboratory.

[13] Chakrabarti, S., 1994. *Offshore Structure Modeling*. World Scientific.

[14] Gopalkrishnan, R., 1993. "Vortex-Induced Forces on Oscillating Bluff Cylinders". PhD thesis, Massachusetts Institute of Technology.

[15] Pontaza, J. P., Baar, J., and Liu, N., 2015. "Vortex-induced motions of a model scale column stabilized floater with round columns in calm water and random waves". *In Proceedings of OMAE2015, May 31June 5, St. John's, Newfoundland, Canada*.